Bulletin of the Seismological Society of America, Vol. 97, No. 1B, pp. 222–233, February 2007, doi: 10.1785/0120060035

Seismogram Envelope Inversion Using a Multiple Isotropic Scattering Model: Application to Aftershocks of the 2001 Bhuj Earthquake

by Simanchal Padhy, U. Wegler, and M. Korn

Abstract We apply the energy transfer theory of 3D multiple isotropic scattering to analyze seismogram envelopes of the 2001 Bhuj earthquake of India. We synthesized the *S*-wave coda envelopes by using a numerical Monte Carlo method. Our model is described by total scattering coefficient g, intrinsic absorption coefficient b, spectral source energy S, and site factors Z. Isotropic source radiation and acoustic wave propagation were assumed. We inverted the observed coda envelopes of 10 aftershocks ($M_L \geq 4$) using the grid search for g, least-squares inversion for b, and S between 1 and 24 Hz. Parameter g does not show significant frequency dependency and averages to 0.01 1/km. This corresponds to a mean free path of 100 km. Parameter b shows weak frequency dependency, increasing with frequency. Its value ranges from 0.02 1/sec to 0.05 1/sec. Consequently, the frequency dependency of intrinsic attenuation takes the power-law form of $Q_i(f) = 280f^{0.72}$. The source energy is largely consistent with the well-known ω^2-source model and the seismic moment is comparable to estimates using standard empirical relations between seismic moment and local magnitude. We also inverted the envelopes for site-amplification factors Z. The values of Z range from 0.5 to 1.75 with no clear frequency dependence, which is consistent with the geology of the region, as the stations were deployed on hard-rock sites.

Introduction

Observed seismograms in high frequencies (>1 Hz) contain information on source, path, and site, but propagation of seismic waves in random heterogeneous medium is mostly path effect. Study of these high-frequency wave propagations in Earth's crust is a complex problem. The complexity stems from the heterogeneity of the crust, which involves numerous physical phenomena like reflection and refraction from velocity discontinuities and multiple scattering. The waves scattered on heterogeneities randomly distributed in the lithosphere interfere incoherently at the receivers forming coda waves. These waves are sensitive to the details of seismic source and the Earth's structure. We cannot evaluate these effects accurately from specific seismic phases, such as direct *P* and *S* waves. On the other hand, to exploit the potential sensitivity of these waves to the details of seismic source and wave path, one must analyze the coda waves. The phase of coda waves is more or less random. Their envelopes exhibit smooth variations depending on frequency and distance. Therefore the seismogram envelopes instead of amplitudes are generally used to understand the random inhomogeneities in the Earth's lithosphere and estimate its properties.

Various approaches have been developed to model envelope shapes in random media. Among them are single-scattering Born theory (Sato, 1977), energy-flux model (Frankel and Wennerberg, 1987; Korn, 1993), Markov approximation (Williamson, 1972; Sato and Fehler, 1998; Saito *et al.*, 2002; Korn and Sato, 2005), and radiative transfer theory (RTT) (Shang and Gao, 1988; Zeng *et al.*, 1991). RTT was at first heuristically derived, but can also be derived directly from the acoustic wave equation (Ishimaru, 1978). Numerical solutions of RTT by the Monte Carlo (MC) method have been developed by Hoshiba (1991), Gusev and Abubakirov (1987), and Yoshimoto (2000). For strong scattering the equation of radiative transfer reduces to the diffusion equation, which can be solved analytically. It was used to explain the late coda of local earthquakes (Margerin *et al.*, 1998) and seismograms recorded on volcanoes (Wegler, 2003).

Most of the models described earlier are based on acoustic wave propagation, that is conversions between *P* and *S* energy are neglected. MC simulations for elastic waves including conversion scattering have been developed by Margerin *et al.* (2000) and Przybilla *et al.* (2006).

Lacombe *et al.* (2003) used acoustic RTT to separate scattering attenuation from intrinsic absorption from L_g coda decay in central France. Bianco *et al.* (2002) investigated the intrinsic dissipation and scattering properties of the litho-

sphere under the Southern Apennines, Italy, in 1- to 12-Hz range. Their result shows that scattering Q^{-1} obtained using multiple-lapse time window (MLTW) analysis under the assumption of a uniform medium is overestimated.

Margerin *et al.* (1999) have used models with depth-dependent velocity and scattering properties to evaluate crustal mean free path and intrinsic Q in Mexico. Husker *et al.* (2006) have inverted *P*- and *S*-wave spectra in the Los Angeles basin for source, path, and site using a standard ω^2-source model (Aki and Richards, 1980, pp. 823) and non-isotropic source radiation. Recently, Sens Schönfelder and Wegler (2006) inverted the envelopes of regional events recorded by the German Regional Seismic Network simultaneously for source, path, and site.

Regarding attenuation studies in India, Singh *et al.* (2004) analyzed the spectral attenuation of L_g waves to determine Q of the Indian shield and have found that $Q_{Lg}(f) = 800f^{0.42}$ between 1 and 20 Hz. Bodin *et al.* (2004) studied the excitation, propagation, and site effects in the Kutch basin of India by using ground-motion recordings and found low attenuation in Kutch, similar to other continental intraplate areas, such as central and eastern North America (ENA). On the basis of ground-motion studies and a comparison of the isoseismal distribution Hough *et al.* (2002) showed that New Madrid and Bhuj regions are characterized by similar propagation characteristics. Iyengar and Raghukanth (2004) also showed similarities in the attenuation relations between Peninsular India and ENA from strong motion records. Padhy (2005) has estimated both intrinsic and scattering attenuation for different tectonic settings assuming a simple Gaussian distribution for the heterogeneities.

Here we present a new method to estimate the effects of source, site, and path from inversion of coda envelopes assuming multiple isotropic scattering of acoustic waves in 3D infinite space with isotropic source radiation based on RTT, where we take into account the full seismogram envelope. The inversion uses grid search over the model space for scattering coefficient, and least-squares inversion for intrinsic absorption coefficient, source energy, and site response. We apply this method to a data set from aftershocks of the Bhuj, India, earthquake in 2001.

Seismological Background and Geological Setting

On 26 January 2001, the Gujarat province in Western India suffered the catastrophic (M_w 7.6) Bhuj earthquake. The mainshock occurred in the Kutch Rift Basin (KRB), which is underlain by a Mesozoic rift system in the western margin of the peninsular India craton. The surface geology of the 2001 earthquake epicentral region comprises Mesozoic (245 to 65 million years old) sediments overlying an uplifted granitic basement. The region lies outside the basalt-covered areas of southern Kutch, which are part of the 65- to 60-million-year-old Deccan traps, one of the largest volcanic provinces in the world. The area has witnessed several historical large earthquakes in the past (Gupta *et al.*, 2001). This pronounced seismicity prompts a need for better understanding of the propagation characteristics of high-frequency seismic waves.

Figure 1 shows the seismicity of the region with locations of the epicenter, aftershocks, and seismic stations used in this study. The Bhuj earthquake was the largest instrumentally recorded intraplate earthquake in the stable continental region of peninsular India. Such earthquakes are rare, accounting for less than 0.5% of global seismicity (Johnston, 1993). Understanding the attenuation properties of high-frequency seismic waves in such a tectonic setting enhances our understanding of the propagation characteristics of the earth medium. Estimating the site amplification is essential for hazard assessment in northwest India, and the results may be compared with other continental intraplate earthquake regions, in particular, the New Madrid Seismic Zone (NMSZ) in the central United States.

The Global focal mechanism solution of the Bhuj earthquake strike 65°, dip 50°, and slip 50° indicates reverse faulting with nodal planes striking about east–west and dipping north–south (Global Centroid Moment Tensor [CMT] Project Catalog; Antolik and Dreger, 2003) (Fig. 1). This is consistent with north–south compression within the Indian Plate (Talwani and Gangopadhyay, 2001). Bodin and Horton

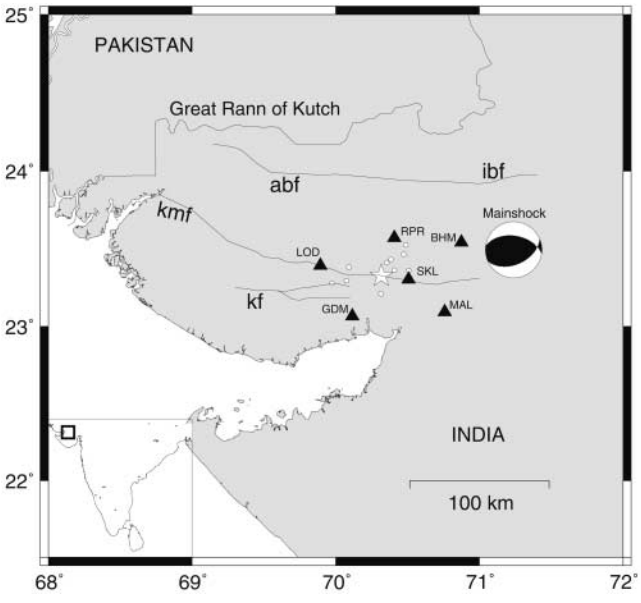

Figure 1. Map of the region around the 2001 Bhuj earthquake. Star represents the hypocenter of the mainshock. The small shaded area in the inset represents the study area. Triangles are the locations of the stations: Rapar (RPR), Samkhyali (SKL), Gandhidham (GDM), Lodai (LOD), Malia (MAL), and Bhimasar (BHM). The epicenters of the aftershocks used in this study, determined with data from a local network set up by NGRI, are shown as small circles. The tectonic features are: ABF, Allah Bund fault; IBF, Island Belt fault; KF, Katrol fault; and KMF, Kutch Mainland fault. The focal mechanism of the mainshock is shown in the right side of the figure.

(2004) have studied in detail the source parameters and tectonic implications of the 2001 Bhuj aftershocks. Their study shows that the aftershock activity is concentrated on a nearly east-striking, south-dipping plane. The aftershocks extend through almost the entire crust.

Data

The data analyzed consists of ten aftershocks ($M_L \geq 4$ with a high signal-to-noise ratio (SNR > 4) recorded at six stations, temporarily deployed in the epicentral region of Bhuj earthquake (Fig. 1) between February and April 2001 by National Geophysical Research Institute (NGRI). The events analyzed are listed in Table 1. Five stations were equipped with short-period L4–3D three-component, 1-Hz velocity seismometers (flat velocity response between 1 and 50 Hz) and one station was equipped with broadband CMG-40T three-component velocity seismometer (flat velocity response between 0.03 and 50 Hz). These stations recorded data in continuous mode at 100 samples per second and with 24-bit resolution. Focal depths of the aftershocks vary from 15 to 36 km. The epicentral distances of the earthquakes range from 10 km to 100 km. The earthquakes were located using HYPO71 (Lee and Lahr, 1975) with the crustal velocity model of (Gupta *et al.*, 2001). All the events were located by more than six stations with horizontal uncertainty (erh) <0.5 km, depth uncertainty (erz) <1 km, and root mean squared travel time residual (rms) 0.02 sec to 0.1 sec. The local magnitudes M_L of the earthquakes were determined using HYPO71 (Lee and Lahr, 1975) with the same velocity model. Determination of M_L is based on the amplitude recorded by a Wood–Anderson torsion seismograph with a natural period of 0.8 sec, a damping constant 0.8, and a static magnification of 2800. The velocity seismograms are used to simulate a Wood-Anderson seismograph (Kanamori *et al.*, 1999), and the peak ground motion was measured from the two horizontal components.

The data processing for generating the coda envelopes includes the following steps:

1. Visual inspection of the data with signal-to-noise ratio (SNR > 4) to discard noisy records.
2. Removal of instrument responses to achieve true amplitude velocity seismograms between 1 and 24 Hz.
3. Filtering with Gaussian bandpass filters with normalization given by

$$\int_{-\infty}^{\infty} |B(T)|^2 dT = 1,$$

where $B(T)$ is the impulse response of the bandpass filter with center frequencies 1.5, 3, 6, 12, and 24 Hz and respective bandwidths 1–2, 2–4, 4–8, 8–16, and 16–32 Hz, and

4. Calculation of energy envelopes of the total wave field, $E_k(r_j, t)$ for the kth event from the three-component sum of mean-squared bandpass-filtered velocity seismogram $\dot{u}\ (r_j, t)$ recorded at receiver r_j using the following relation.

$$E_k\ (r_j,\ t) = \rho_0 \left[\frac{\dot{u}^2\ (r_j,\ t) + H^2\ (\dot{u}\ (r_j,\ t))}{2} \right] \qquad (1)$$

where dot ($\cdot$) represents time derivative, ρ_0 is the mean density of the medium, and H denotes Hilbert transform. We have used $\rho_0 = 2500$ kg/m^3.

Modeling and Inversion

Radiative Transfer Equation for Acoustic Waves

In this section we present the physical properties of the multiple scattering model, and explain our numerical scheme to solve the radiative transfer equation for acoustic waves. As explained above, we have considered a simple model of multiple scattering in a unbounded 3D full space assuming isotropic source radiation and isotropic scattering, and consisting of a homogeneous constant-velocity background me-

Table 1
List of All Earthquakes and Their Parameters Used in This Study

Event No.	Date (dd:mm:yy)	Time (UTC) (hh:mm:ss)	Depth (km)	Latitude (deg)	Longitude (deg)	M_L	M_{emp} (N m)	M_{obs} (N m)
01	07:02:01	10:30:54.91	21.93	23.346	70.401	4.3	1.41×10^{15}	1.83×10^{15}
02	08:02:01	03:25:55.44	16.95	23.269	70.323	4.2	1.0×10^{15}	1.02×10^{15}
03	08:02:01	09:32:12.53	26.33	23.438	70.502	4.5	2.82×10^{15}	2.75×10^{15}
04	08:02:01	14:12:17.9	29.21	23.395	70.287	4.4	1.99×10^{15}	0.9×10^{15}
05	08:02:01	16:54:41.82	28.02	23.715	70.443	4.0	0.5×10^{15}	1.15×10^{15}
06	09:02:01	10:07:41.26	35.64	23.24	70.01	4.0	0.5×10^{15}	0.75×10^{15}
07	09:02:01	12:37:03.21	16.20	23.267	70.32	4.5	2.82×10^{15}	1.19×10^{15}
08	10:02:01	05:37:32.9	23.97	23.658	70.483	4.0	0.5×10^{15}	0.28×10^{15}
09	10:02:01	19:30:57.41	29.93	23.38	70.092	4.4	1.99×10^{15}	1.77×10^{15}
10	11:02:01	02:33:21.37	15.46	23.431	70.566	4.3	1.41×10^{15}	1.1×10^{15}

dium with random inhomogeneities. The acoustic radiative transfer equation for such a medium is given as follows (Chandrasekhar, 1960; Ishimaru, 1978; Van de Hulst, 1980; Rytov *et al.*, 1987; Apresyan and Kravtsov, 1996).

$$\frac{1}{v}\,\partial_t W(\vec{x},\,t,\,\hat{\vec{k}}) \;+\; \hat{\vec{k}}\;\vec{\nabla}_x W(\vec{x},\,t,\,\hat{\vec{k}}) = \;-g_0(f)W(\vec{x},\,t,\,\hat{\vec{k}}) \;+\; \frac{1}{4\pi}\int g\,(\hat{\vec{k}},\,\hat{\vec{k}}')W(\vec{x},\,t,\,\hat{\vec{k}}')d\hat{\vec{k}}' \;+\; e(\vec{x},\,t,\,\hat{\vec{k}}) \qquad (2)$$

where W is the intensity or average squared wave field, which is the amount of energy flowing across a surface in a specified direction per unit time, per unit solid angle, and per unit surface. It is a function of the position, $\vec{x}$; the time of observation, t, and a unit vector in the direction of propagation, $\hat{\vec{k}}$. Operator ∇_x denotes derivatives with respect to $\vec{x}$. Due to the presence of heterogeneities, a wave with wave vector $\vec{k}'$ at a point $\vec{x}$ may be scattered into any direction $\hat{\vec{k}}$ with wave vector $\vec{k}$. The parameter $g(\hat{\vec{k}},\,\hat{\vec{k}}')$ is the differential scattering cross section between the incoming wave with wavenumber vector $\vec{k}'$ and the scattered wave with wavenumber vector $\vec{k}$. The parameter $g_0(f)$ is the total scattering coefficient obtained by integrating $g(\hat{\vec{k}},\,\hat{\vec{k}}')$ over all directions $\hat{\vec{k}}'$, as defined later in this section, e is the source term, and v is S-wave velocity. The left-hand side of equation (2) is the variation of energy during propagation along $\hat{\vec{k}}$. On the right-hand side, loss and gain mechanisms in addition to sources determine the dynamic behavior. The first term on right-hand side is the energy loss of incident beam in all directions due to scattering. The second term represents the reinforcement of incident beam due to scattered energy from direction $\vec{k}'$ to direction $\vec{k}$. This equation expresses the local conservation of energy. As defined earlier, the total scattering coefficient obtained on integrating $g(\hat{\vec{k}},\,\hat{\vec{k}}')$ over all directions $\hat{\vec{k}}'$, is given by the following expression.

$$g_0(f) \;=\; \frac{1}{4\pi}\int g(\hat{\vec{k}},\,\hat{\vec{k}}')d\hat{\vec{k}}' \;=\; \frac{1}{l} \qquad (3)$$

where l is the scattering mean free path in kilometers. For isotropic scattering as discussed in the present study, $g(\hat{\vec{k}},\,\hat{\vec{k}}') \;=\; g_0$. Integration of $W(t,\,\vec{x},\,\hat{\vec{k}})$ over all directions $\vec{k}$ gives the theoretical energy envelope,

$$E_G(r_j,\,t_i;\,g) \;=\; \frac{1}{v}\int W\,(t,\,\vec{x},\,\hat{\vec{k}})\,d\hat{\vec{k}}, \qquad (4)$$

where $E_G(r_j,\,t_i;\,g)$ is the energy density Green's function at distance r_j and at time t_i, which depends only on g.

We have synthesized the seismogram envelopes for the local earthquakes assuming the multiple isotropic scattering model based on RTT. RTT was solved numerically using the MC method to calculate the coda envelopes. The MC envelopes were convolved with Gaussian filters with central frequencies at 0 Hz and bandwidths of 0.25, 0.5, 1.0, 2.0, and 4.0 Hz to smooth the envelopes calculated for 1.5, 3, 6, 12, and 24 Hz, respectively.

Monte Carlo Method

We solved the acoustic radiative transfer equation (2) numerically by the Monte Carlo method following the method of Gusev and Abubakirov (1996) and Yoshimoto (2000). The central characteristic of MC methods is to simulate the behavior of one energy particle at a time. The average over a large number of realizations of particle paths yields an estimate of the particle probability density and is interpreted as the energy radiated from the source. Let each particle have unit energy.

At the source, each particle is shot with takeoff angle θ, azimuth ϕ at the origin determined by the following relations and with a velocity in random direction for an isotropic source:

$$\theta \;=\; \arccos(1 \;-\; 2U_1),\; \phi \;=\; 2\pi U_2 \qquad (5)$$

where U_1 and U_2 are uniform random variables between 0 and 1. Equation (5) ensures uniform probability distribution of the shooting direction. During propagation the particle is characterized by the time it has already traveled, its position, and its current direction of propagation. The MC method propagates each particle with a fixed, small time interval, Δt relative to the average mean free time of a particle in the medium, given by

$$v\Delta t \ll \frac{1}{g_0} \;=\; l. \qquad (6)$$

The mean free path l is the reciprocal of total scattering coefficient g_0. Next we examined whether the particle scattered within Δt, which was decided by a random process. For each timestep a random variable U_3 was computed with equal distribution between 0 and 1. If $U_3 < v\Delta t/l$ is satisfied, scattering takes place. At each timestep, it was checked whether the particle was within a small receiver volume. Because of the assumption of isotropy, the receiver volume was considered as a spherical shell. All particles, which were in a certain timestep within the receiver volume, were added up. The energy density at the receiver at time t was evaluated as $n(t)/(N\,\Delta V)$, where $n(t)$ is the number of particles included in the receiver volume ΔV, and N is total number of particles shot. We referred to the time history of the seismic energy density at the receiver as seismogram envelope. The parameters used in simulation were as follows: $N \;=\; 10^6$, $\Delta t \;=$

0.1 sec, which is roughly one hundredth of the mean free time.

Inversion

For the inversion, we assume an isotropic source in infinite homogeneous medium, in which isotropic scatterers are distributed in a uniformly random manner. Two parameters namely scattering coefficient and intrinsic absorption of *S* waves, characterize the medium. The scattering coefficient represents the scattering power per unit volume.

Coda waves that have left the seismic source with all possible direction give a good estimate of the total energy emitted at the source, independent of station location. Coda waves, in essence a multiple-scattering process, homogenize the spatial distribution of energy. On this basis, energy spectral density $E_k(r_j, t_i; f)$ observed for event k at receiver j and at lapse time t_i is given by

$$E_k(r_j, t_i; f) = Z_j(f) S_k(f) E_G(r_j, t_i; g, f) e^{-bt_i} \quad (7)$$

where Z_j is the site factor for the jth station, S_k is the source factor for the kth event, b represents intrinsic attenuation coefficient measured in 1/sec, and f is frequency. $E_k(r_j, t_i; f)$ is represented by the bandpass-filtered observed envelope. $E_G(r_j, t_i; g, f)$ is the spectral estimate of energy density Green's function at distance r_j and at time t_i, which depends only on g. It is numerically computed using the MC method based on RTT. As E_G is derived for an infinite homogeneous medium, its amplitude is multiplied by 4 ($= 2^2$) as a correction for a free-surface amplification for energy density. A time window starting from the *S*-wave onset to the lapse time (up to 300 sec) until it reached four times noise level was used in inversion.

The inversion was performed in two steps. In the first step, inversion was carried out to separate the source and attenuation effects without considering site. In the second step, inversion was carried out for the site functions using the observed data that have been corrected for the source and attenuation results.

We used a grid search method to estimate the most appropriate value of g. The values for g were searched in the range between 0.001 and 0.05 with 100 increments over the entire model space. We then iteratively estimated the unknown values of b, and S_k from the following equation using the χ^2 least-squares fitting:

$$\ln\left[\frac{E_k}{E_G}\right] = \ln[S_k] - bt_i \,. \quad (8)$$

We have not considered the site effect in this step. We have fitted the theoretical envelope E_G for a given model to the observed envelope E_k to minimize the residual between them in the following least-squares sense:

$$\chi^2 = \sum_{k=1}^{N} \left(\ln[E_k(r_j, t_i; f)] - \ln[E_G(r_j, t_i; g, f)]\right)^2 \rightarrow \text{Min.} \quad (9)$$

In the second step, for estimation of site-amplification factor Z_j, we rearranged equation (7) as

$$E_k(r_j, t_i; f) = Z_j(f) E_G(r_j, t_i; g, f) e^{(-bt_i + \ln S_k)}$$
$$\Rightarrow \ln Z_j = \sum_k \left[\ln\left(\frac{E_k}{E_G}\right) + bt_i - \ln S_k\right] \quad (10)$$

The site factor Z_j for each station j was obtained from inversion for fixed values of S_k, b, and g of the best-fitting model from the logarithmic averages of Z_j values based on equation (10). All events, recorded at a given site for a particular frequency were used for computing average site factor and its error bars. Then site factor Z was computed for all central frequencies (1.5, 3, 6, 12, and 24 Hz) following the same procedure.

Results

Computation of Medium Parameters

Figure 2 shows the comparison of the observed and synthesized envelopes for one event (Event 9 of Table 1) at 3 Hz central frequency. It exhibits a reasonably good fit, except for station SKL. The degree of misfit at station SKL may be attributed to the effects of site amplification, which is described later in this section. The model parameters obtained from inversion of all ten events were plotted as a function of frequency in Figure 3a–c. Slight misfit near direct *S* wave for stations RPR and BHM as shown in Figure 2 may be due to the effect of source radiation. Parameter g varies between 0.003 l/km and 0.04 l/km, with an average value of 0.01 l/km, which corresponds to mean free path of 100 km. No clear frequency dependency is observed. Such a variation in value of mean free path may be associated with possible trade-offs inherent to the inversion methodology. However, to a first-order approximation, we can say the average value of g as 0.01 l/km, which corresponds to mean free path of 100 km. For a shear-wave velocity of 3.3 km/sec in the crust, this implies a scattering mean free time of only 30 sec, much smaller than the observed duration (up to 300 sec) of the coda. This supports the view that seismic coda consists of multiple-scattered energy. The value of intrinsic attenuation coefficient b shows weak frequency dependency, increasing with frequency (Fig. 3b). It ranges from 0.02 l/sec to 0.05 l/sec. However, as our model considers a homogeneous background medium, the estimates of intrinsic attenuation can be overestimated. Intrinsic attenuation, ($Q_i^{-1} = b/2\pi f$), scattering attenuation ($Q_s^{-1} = gv/2\pi f$), and total attenuation ($Q^{-1} = Q_i^{-1} + Q_s^{-1}$) are shown in Figure 3c. The total attenuation shows high value at low frequencies and decreases with frequency. The frequency-dependent power

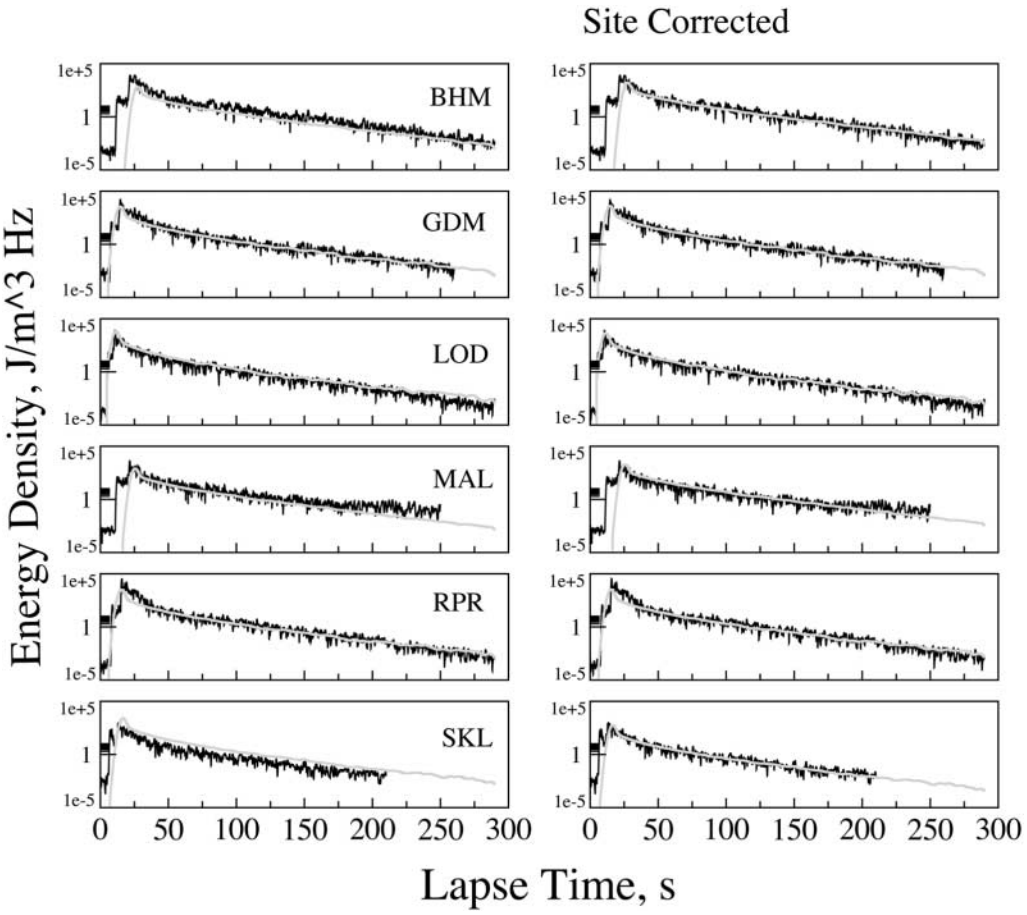

Figure 2. Comparison between the observed (black curve) and the synthesized envelopes (gray curve) at 3 Hz for event 9 of Table 1 without (left) and with (right) site correction applied. Synthesized envelopes calculated with best-fit model parameters fit reasonably well to observed ones. Site correction is significant only for station SKL.

law forms of intrinsic, scattering, and total attenuations were found as $(280 \pm 24)f^{0.72\pm0.02}$, $(150 \pm 35)f^{0.95\pm0.01}$, and $(98 \pm 26)f^{0.85\pm0.02}$, respectively. The errors in coefficients and exponents are estimated at the one standard deviation (1σ) level. The power law exponent for scattering attenuation Q_s is 0.95, which shows almost frequency-independent behavior of g as shown in Figure 3a. However, because of the possible trade-off inherent to any inversion method, it is difficult to discuss more on frequency dependence and dominance of intrinsic or scattering attenuation.

Source Displacement Spectrum

Sens Schönfelder and Wegler (2006) compared the low-frequency limit of seismic-moment spectra with seismic moments estimated from coda inversion techniques. They found excellent agreement. In the present study, the spectral estimates of source energies for each event resulting from inversion were used to estimate the source spectrum $M(\omega)$ using the following relation for the S-wave source energy spectral density (Sato and Fehler, 1998, p. 152).

$$S_i(\omega) = \frac{\omega^4 |M_i(\omega)|^2}{10\ \pi\rho_0\beta_0^5} \tag{11}$$

Here ρ_0 is density of crustal rocks 2500 kg/m^3, β_0 is S-wave velocity 3.3 km/sec, and $M(\omega)$ is the Fourier transform of the seismic-moment time function.

Next, we have empirically derived the source spectrum by assuming the ω^2-source model (Aki and Richards, 1980, p. 823):

$$\omega|M(\omega)| = \frac{M_0}{1 + \left(\frac{\omega}{\omega_c}\right)^2} \tag{12}$$

Seismic-moment M_0 and corner frequency $f_c = \omega_c/2\pi$ are determined from local magnitude M_L using the empirical relations $\log M_0(\text{N m}) = 1.5M_L + 8.7$ (Peishan and Haitong, 1989) and $\log f_C = 1.5 - 0.2M_L$ (Watanabe, 1971). The observed and empirically derived source-displacement spectra are shown in Figure 4 with thick and thin curves,

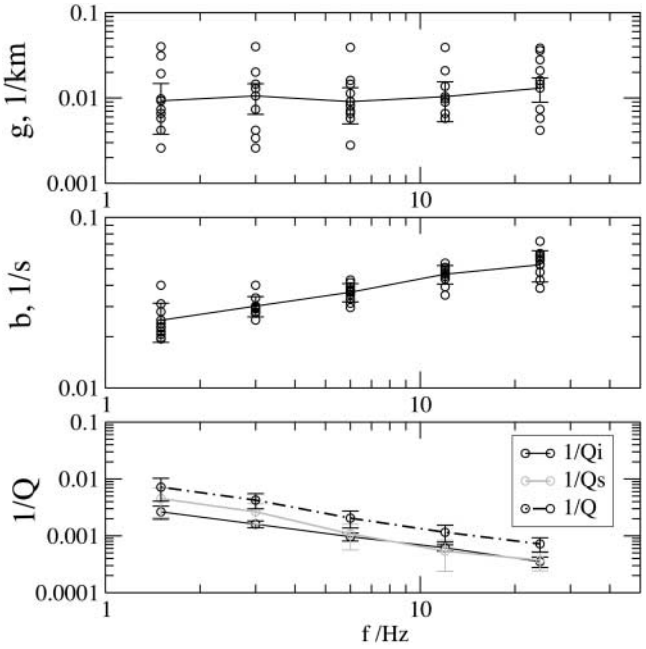

Figure 3. Frequency dependence of scattering coefficient, g (a), intrinsic attenuation coefficient, b (b), and $1/Q$ for scattering, intrinsic, and total attenuation (c). The error bars represent one standard deviation level.

respectively. The spectral shape is largely consistent with the ω^2-model. Only events 4 and 7 show a faster decay than ω^{-2}. The spectral level at low frequencies gives an estimate of the seismic moment M_0. The seismic moment estimated from the low-frequency portion of the curves (marked by small horizontal lines) shown in Figure 4 are in agreement with the empirically estimates within error limits except for events 4 and 7 with offset between the two, where the decay of source spectrum is faster than predicted by the ω^2-source model. This offset is also explained by many workers (Boatwright, 1978; Fletcher, 1980; Dysart *et al.*, 1988), who have claimed that neither ω^2 nor ω^3 is appropriate to describe the observations. Wang and Huang (2004a) have shown that for large events ($M_L > 4$), the earthquake source spectra decay at a faster rate $\omega^{-2.5}$ at higher frequencies. Table 1 shows the observed and predicted values of seismic moments for each event. The observed $M(\omega)$ agrees not too badly with the ω^2 model and moment estimates from magnitudes. Disagreement between spectral shape can be attributed to inappropriateness of the ω^2-model. Discrepancies in the moment estimate may come from the inadequacy of empirical moment-magnitude relations, and of regional attenuation characteristics. Other factors like inaccuracy of local magnitude determination, possible ambiguities in source/path trade-offs, source radiation pattern, and underestimate of source energies due to finite-frequency bandwidth effect (Wang and Huang, 2004b) may also contribute to the observed discrepancies. However, the main advantage of our method is (1) in the moment determination, which can be done without having to determine local magnitudes, and (2) in extracting the information about the medium without normalizing to a common source and site. Thus, this method may be more stable than other approaches like coda normalization method as have been used in many of the earlier studies.

Site Effects

Figure 5 shows site factor Z as a function of frequency for all stations. The uncertainties in site factors shown in Figure 5 are at 1σ level. In most cases, Z is close to unity and shows no significant dependency on frequency. This result is consistent with the geology of the region, as most of the stations were placed on hard rock sites. Only for station SKL an average site factor of 0.67 was found over the entire frequency range of 1–24 Hz. This is evident from Figure 2, where the poor level of fitting of theoretical and observed envelope for station SKL is improved after taking care of the site effect.

Discussion

Comparison with Other Intraplate Tectonic Settings

We compare our results for scattering and intrinsic attenuation with those obtained in various intraplate regions by applying largely similar methods. Table 2 compares our results with those of others.

As shown by several authors (Margerin *et al.*, 1999; Hoshiba *et al.*, 2001; Lacombe *et al.*, 2003), the stratification of heterogeneity and of the background medium play an important role in the interpretation of coda waves. Lacombe *et al.* (2003) analysed L_g coda envelopes of regional events in central France assuming a crustal layer over a half-space. They observed a strong trade-off between g and b and therefore were not able to reliably conclude on the dominance of intrinsic or scattering attenuation. Margerin *et al.* (1999) determined coda-Q parameter from local earthquakes in Mexico assuming a heterogeneous and scattering crust overlying a homogeneous mantle. They showed the effect of energy leakage at the base of the crust into the mantle on coda-Q, intrinsic and scattering attenuations. Recently, Sens Schönfelder and Wegler (2006) studied the scattering characteristics of the lithosphere for Germany using the acoustic RTT for the multiple isotropic scattering model. They found an average mean free path of 690 km and average intrinsic attenuation $Q_i = 500$ below 3 Hz.

Many authors investigated intrinsic and scattering attenuation of the lithosphere using the MLTW analysis applied to the coda of the local earthquakes under the assumption of uniform distribution of scatterers and isotropic scattering. For example, Bianco *et al.* (2002) for Southern Apennines, Italy; Hoshiba (1993) for Japan; Jin *et al.* (1994) for southern California; and Mayeda *et al.* (1992) for central California, Long Valley, and Hawaii. Hoshiba *et al.* (2001) extended MLTW analysis to a depth-dependent velocity structure and

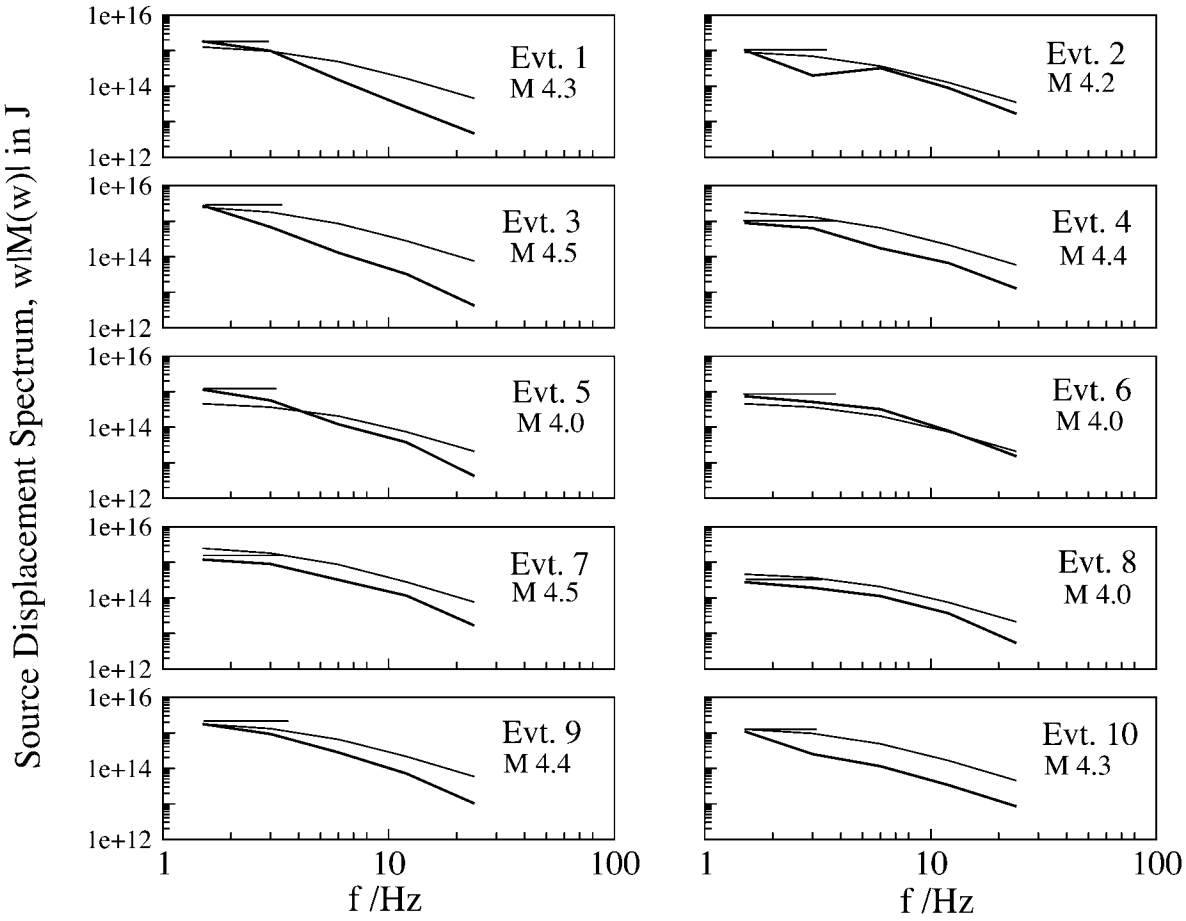

Figure 4. Source-displacement spectra obtained by the observation (thick curve) and by the empirical relation between local magnitude and energy (thin curve) for all ten events used in this study. The constant low-frequency estimate of the spectra represented by small horizontal line yields the value of seismic moment. The event number and magnitude mentioned on each plot correspond to those of Table 1.

applied it to the coda of local earthquakes in northern Chile. They found that scattering attenuation is comparable to or smaller than intrinsic absorption between 1 and 8 Hz.

Our present analysis is based on the modeling of coda waves with RTT based on homogeneous properties of the background and scattering medium, which neglects the guiding of seismic waves in the crust. The average mean free path is of the order of 100 km and mean free absorption path varies between about 70 km and 170 km depending on frequency. The values of b of our study are larger than those of Margerin *et al.* (1999), Hoshiba *et al.* (2001), and Lacombe *et al.* (2003). Our estimate of Q_i may be overestimated because of the hypothesis of a homogeneous background medium. However, the values of g are smaller than their estimates. Our estimates of g are underestimated, which may be due to large forward scattering at high frequencies. On the other hand, our estimates of g and Q_i are more or less in the same range of those of Bianco *et al.* (2002), Mayeda *et al.* (1992), Jin *et al.* (1994). The values of scattering coefficient of all these studies, who assume a uniform medium, are probably overestimated.

Thus the observed differences in medium parameters (Table 2) from all these studies may be attributed to the methodology, the error estimates, and the regional variations. For example, most of the studies mentioned previously computed error levels at 95% confidence levels. However, we calculated errors at 1σ level and so on.

Attenuation studies in India mostly includes attenuation of (1) coda waves of local earthquakes in Garhwal Himalaya (Gupta *et al.*, 1995), in northwest Himalaya (Kumar *et al.*, 2005), Koyna (Gupta *et al.*, 1998; Gupta and Kumar, 2002) using a single-scattering model, (2) *Lg* waves in Indian shield (Singh *et al.*, 2004) using data from 1997 Jabalpur, 2001 Bhuj, 1999 Chamoli, and 1991 Uttarkashi earthquakes in distance range of 240–2400 km using a stochastic method. The attenuation of coda waves Q_C^{-1} for Himalaya, Koyna, and northeast India are similar to Q_S rather than Q_i (Table 2). This indicates a similar nature of heterogeneities in these regions. Singh *et al.* (2004) found $Q_{Lg}(f) = 800f^{0.42}$ in 0.1–20 Hz and showed that the estimates of Q of both the Indian shield and ENA are similar. Our results differ from those of Singh *et al.* (2004) in the nature of the data analyzed. As we

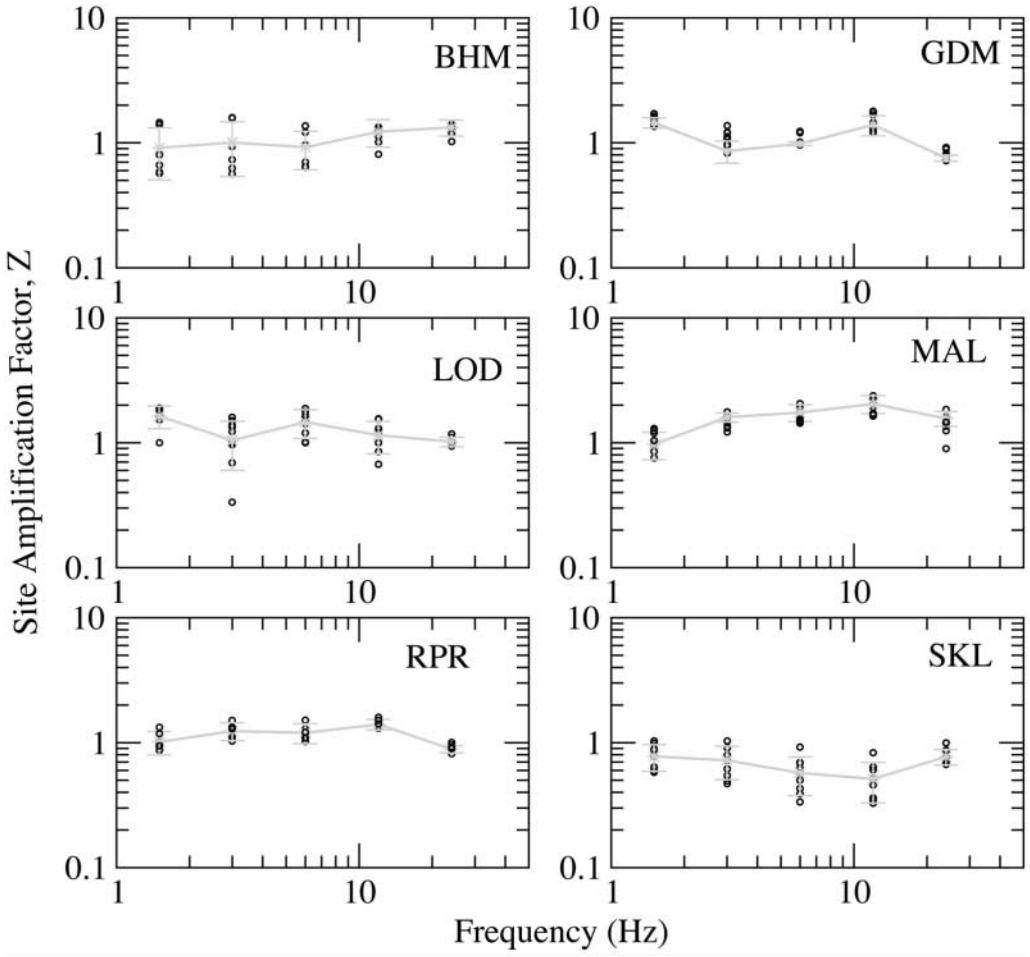

Figure 5. Site-amplification factors for *S*-wave amplitude recorded at different stations. Estimated factors range between 0.5 and 1.75 for most stations. The circles represent individual events, and starts represent the average. The error bars represent one standard deviation level.

do not have any evidence of individual estimates of scattering attenuations and intrinsic absorptions in these regions, we cannot compare our results in detail with those of previous studies with regard to their medium properties.

Depth Dependence of g and b

Although the spatial uniformity in g and b are assumed in this analysis, they may in reality depend on depth. It is reasonable to consider changes in values of g and b across Moho discontinuity, as pointed out by Fehler *et al.* (1992). This discontinuity is not taken into account in this study. The density of scatterers may decrease with depth, which leads to a decrease in g with depth. In case of depth dependency, the results may depend on the difference of focal mechanism, and focal depth of the events. If strong reflected waves are observed in coda waves as described in Obara and Sato (1988), we cannot directly apply this method. Hoshiba (1993) and Hoshiba *et al.* (2001) have analyzed the coda waves for the layered structure. Therefore, it would be necessary to extend the multiple scattering model to depth-dependent layered media, so that we will be able to find the spatial variations in g and b.

In summary, the discrepancies in estimates of scattering and intrinsic attenuations of different studies are mainly attributed to differences in methods, model assumptions, regional differences, and also to computation of error bars. Also, methodological shortcomings are possible: like the trade-offs inherent in the inversion methodology used, trade-offs among the various parameters Z versus S, $Z+S$ versus $\{g, b\}$ as mentioned earlier. Our results suggest that for a better understanding of the observed data, a theoretical model should include both a layered velocity structure and a spatially nonuniform distribution of scatterers.

Conclusion

We synthesized coda envelopes using Monte Carlo solutions of the acoustic radiative transfer theory with isotropic scattering coefficients, and fitted them to aftershock data of

Table 2
A Comparative Study of Scattering Attenuation, Intrinsic Absorption, and Total Attenuation and Their Frequency Dependences for Different Regions*

Reference	Region	Frequency Band (Hz)	Mean Free Path (km)	Intrinsic Attenuation (Q_i)	Total Attenuation (Q)
Lacombe *et al.* (2003)	Central France	2–5			
		Crust	30–1000	200–1500	
		Mantle	250–100,000	200–1500	
Margerin *et al.* (1999)	Mexico	1–20	10–100	1000	
Hoshiba *et al.* (2001)	Northern Chile	1–8	122–294	260–1400	140–940
Bianco *et al.* (2002)	Southern Apennine, Italy	1–12	16–53	139–1031	202–22,222
Hoshiba (1993)	Japan	1.5–6	25–928	100–714	36–555.5
Mayeda *et al.* (1992)	Hawaii	1.5–15	19–248	1111–1667	50–1250
	Long Valley		19–62	333–1818	45–714
	Central California		27–74	270–769	63–588
Jin *et al.* (1994)	Southern California	0.5–24	25–67	45–1231	13–862
Sens Schönfelder and Wegler (2006)	Germany	0.2–24	690	500	
This study	Bhuj, India	1.5–24	100	377–2742	138–1460
			$Q_S(f) = 150f^{0.95}$	$Q_i(f) = 280f^{0.72}$	$Q(f) = 98f^{0.85}$
Gupta and Kumar (2002)	Garhwal Himalaya	1–18			$Q_C(f) = 149f^{0.95\dagger}$
	Koyna	1.5–24			$Q_C(f) = 131f^{1.04\dagger}$
	Northeast India	1.5–16			$Q_C(f) = 86f^{1.02\dagger}$
Singh *et al.* (2004)	Indian Shield	$0.1 \le f \le 20$			$Q_{Lg}(f) = 800f^{0.42}$
Kumar *et al.* (2005)	Northwest Himalaya	1–18			$Q_C(f) = 158f^{1.05\dagger}$

*Information not available, spaces are left blank.
†Q_C refers to Coda-Q of coda waves.

the Bhuj 2001 earthquake, India. From the fit, the source, medium, and site parameters have been estimated. We could separate scattering attenuation from intrinsic absorption. The estimated parameters are weakly frequency dependent and exhibit low attenuation character of the medium, which is similar to other intraplate continental settings like eastern/central North America and central Europe. The source energies are grossly compatible with the ω^2-source model for spectral amplitudes. The seismic moments determined from the envelopes are in good agreement with those estimated using standard empirical relations between moment and local magnitude. Thus, a simultaneous inversion of both source and medium parameters is possible using only a sparse network of stations and a few events. The methodology could be used as a standard method with aftershock data in regions that are only monitored by sparse instrumentation.

Acknowledgments

We are grateful to Robert L. Nowack and three anonymous reviewers for their critical comments on improving the study and thereby the manuscript. S.P. acknowledges CSIR-DAAD exchange program, under which this study was carried out. C. Sens Schönfelder is highly acknowledged for his favor in data processing and fruitful discussions during the course of work. Discussions with J. Przybilla are also acknowledged. Figure 1 was generated using Generic Mapping Tools (GMT) (Wessel and Smith, 1995). S.P. thanks K. Mallick for carefully reading the manuscript and V. P. Dimri, Director, NGRI, for his permission to publish this work.

References

Aki, K., and P. Richards (1980). *Quantitative Seismology: Theory and Methods*, W. H. Freeman, San Francisco.

Antolik, M., and D. S. Dreger (2003). Rupture process of the 26 January 2001 M_w 7.6 Bhuj, India, earthquake from teleseismic broadband data, *Bull. Seism. Soc. Am.* **93,** 1235–1248.

Apresyan, L. A., and Y. A. Kravtsov (1996). *Radiative Transfer: Statistical and Wave Aspects,* Gordon and Breach Publishers, Amsterdam.

Bianco, F., E. Del Pezzo, M. Castellano, J. M. Ibanez, and F. DiLuccio (2002). Separation of intrinsic and scattering seismic attenuation in the southern Apennine zone, Italy, *Geophys. J. Int.* **150,** 10–22.

Boatwright, J. (1978). Detailed spectral analysis of two small New York State earthquakes, *Bull. Seism. Soc. Am.* **68,** 1117–1131.

Bodin, P., and S. Horton (2004). Source parameters and tectonic implications of aftershocks of the Mw 7.6 Bhuj earthquake of 26 January 2001, *Bull. Seism. Soc. Am.* **94,** 818–827.

Bodin, P., L. Malagnini, and A. Akinci (2004). Ground-motion scaling in the Kachchh Basin, India, deduced from aftershocks of the 2001 Mw 7.6 Bhuj earthquake, *Bull. Seism. Soc. Am.* **94,** 1658–1669.

Chandrasekhar, S. (1960). *Radiative Transfer*, Dover, New York.

Dysart, P. S., J. A. Snoke, and I. S. Sacks (1988). Source parameters and scaling relations for small earthquakes in the Matsushiro region, southwest Honshu, Japan, *Bull. Seism. Soc. Am.* **78,** 571–589.

Fehler, M., M. Hoshiba, H. Sato, and K. Obara (1992). Separation of scattering and intrinsic attenuation for the Kanto-Tokai region, Japan using measurements of S-wave energy versus hypocentral distance, *Geophys. J. Int.* **108,** 787–800.

Fletcher, J. B. (1980). Spectra from high-dynamic range digital recordings of Oroville, California, aftershocks and their source parameters, *Bull. Seism. Soc. Am.* **70,** 735–755.

Frankel, A., and L. Wennerberg (1987). Energy-flux model of seismic coda: separation of scattering and intrinsic attenuation, *Bull. Seism. Soc. Am.* **77,** 1223–1251.

Global Centroid Moment Tensor (CMT) Project catalog search, www.globalcmt.org/CMTsearch.html (last accessed April 2004).

Gupta, H. K., N. P. Rao, B. K. Rastogi, and D. Sarkar (2001). The deadlist intraplate earthquake, *Science* **291,** 2101–2102.

Gupta, S. C., and A. Kumar (2002). Seismic wave attenuation characteristics of three Indian regions: a comparative study, *Curr. Sci.* **82,** no. 4, 407–413.

Gupta, S. C., V. N. Singh, and A. Kumar (1995). Attenuation of coda waves in the Garhwal Himalaya, *Phys. Earth Planet. Interiors* **87,** 247–253.

Gupta, S. C., S. S. Teotia, S. S. Rai, and N. Gautam (1998). Coda Q estimates in the Koyna region, India, *Pure Appl. Geophys.* **153,** 713–731.

Gusev, A. A., and I. R. Abubakirov (1987). Monte-Carlo simulation of record envelope of a near earthquake, *Phys. Earth Planet. Interiors* **49,** 30–36.

Gusev, A. A., and I. R. Abubakirov (1996). Simulated envelopes of non-isotropically scattered body waves as compared to observed ones: another manifestation of fractal heterogeneity, *Geophys. J. Int.* **127,** 49–60.

Hoshiba, M. (1991). Simulation of multiple-scattered coda wave excitation based on the energy conservation law, *Phys. Earth Planet. Interiors* **67,** 123–136.

Hoshiba, M. (1993). Separation of scattering attenuation and intrinsic absorption in Japan using the multiple time window analysis of full seismogram envelope, *J. Geophys. Res.* **98,** 15,809–15,824.

Hoshiba, M., A. Rietbrock, F. Scherbaum, H. Nakahara, and C. Haberland (2001). Scattering attenuation and intrinsic absorption using uniform and depth dependent model: application to full seismogram envelope recorded in Northern Chile, *J. Seism.* **5,** no. 2, 157–179.

Hough, S. E., S. Martin, R. Bilham, and G. M. Atkinson (2002). The 26 January 2001 M 7.6 Bhuj, India earthquake: observed and predicted ground motions, *Bull. Seism. Soc. Am.* **92,** 2061–2079.

Husker, A. L., D. K. Monica, and P. M. Davis (2006). Anomalous seismic amplitudes measured in the Los Angeles Basin interpreted as a basin-edge diffraction catastrophe, *Bull. Seism. Soc. Am.* **96,** 147–164.

Ishimaru, A. (1978). *Wave Propagation and Scattering in Random Media*, Vols. 1 and 2, Academic Press, New York.

Iyengar, R. N., and S. T. G. Raghukanth (2004). Attenuation of strong ground motion in peninsular India, *Seism. Res. Lett.* **75,** 530–540.

Jin, A., K. Mayeda, D. Adams, and K. Aki (1994). Separation of intrinsic and scattering attenuation in southern California using TERRAscope data, *J. Geophys. Res.* **99,** 17,835–17,848.

Johnston, A. C. (1993). EPRI Report TR 10261, Chap. 3, Electric Power Research Institute, Palo Alto, California,

Kanamori, H., P. Maechling, and E. Hauksson (1999). Continuous monitoring of ground-motion parameters, *Bull. Seism. Soc. Am.* **89,** 311–316.

Korn, M. (1993). Determination of site-dependent scattering Q from P-wave coda analysis with an energy-flux model, *Geophys. J. Int.* **113,** 54–72.

Korn, M., and H. Sato (2005). Synthesis of plane vector wave envelopes in two-dimensional random elastic media based on the Markov approximation and comparison with finite-difference simulations, *Geophys. J. Int.* **161,** 839–848.

Kumar, N., I. M. Parvez, and H. S. Virk (2005). Estimation of coda wave attenuation for NW Himalayan region using local earthquakes, *Phys. Earth Planet. Interiors* **151,** 243–258.

Lacombe, C., M. Campillo, A. Paul, and L. Margerin (2003). Separation of intrinsic absorption and scattering attenuation from L_g coda decay in central France using acoustic radiative transfer theory, *Geophys. J. Int.* **154,** 417–425.

Lee, W. H. K., and J. C. Lahr (1975). HYPO71 (revised): a computer program for determining hypocenter, magnitude, and first motion pattern of local earthquakes, *U.S. Geol. Surv. Open-File Rept. 116*, 75–311.

Margerin, L., M. Campillo, N. M. Shapiro, and B. A. van Tiggelen (1999). Residence time of diffuse waves in the crust as a physical interpretation of coda Q: application to seismograms recorded in Mexico, *Geophys. J. Int.* **138,** 343–352.

Margerin, L., M. Campillo, and B. A. van Tiggelen (1998). Radiative transfer and diffusion of waves in a layered medium: new insight into coda Q, *Geophys. J. Int.* **134,** 596–612.

Margerin, L. , M. Campillo, and B. A. van Tiggelen (2000). Monte Carlo simulation of multiple scattering of elastic waves, *J. Geophys. Res.* **105,** 7873–7892.

Mayeda, K., S. Koyanagi, M. Hoshiba, K. Aki, and Y. Zeng (1992). A comparative study of scattering, intrinsic, and coda Q^{-1} for Hawaii, Long valley, and central California between 1.5 and 15.0 Hz, *J. Geophys. Res.* **97,** 6643–6659.

Obara, K., and H. Sato (1988). Existence of an S wave reflector near the upper plate of the double seismic zone beneath southern Kanto district, Japan, *J. Geophys. Res.* **93,** 15,037–15,045.

Padhy, S. (2005). A scattering model for seismic attenuation and its global applications, *Phys. Earth Planet. Interiors* **148,** 1–12.

Peishan, C., and C. Haitong (1989). Scaling law and its applications to earthquake statistical relations, *Tectonophysics* **166,** 53–72.

Przybilla, J., M. Korn, and U. Wegler (2006). Radiative transfer of elastic waves versus finite difference simulations in two-dimensional random media, *J. Geophys. Res.* **111,** B04305, doi 10.1029/2005JB003952.

Rytov, S. M., Y. A. Kravtsov, and V. I. Tatarskii (1987). *Principles of Statistical Radio Physics*, Vol. 4. *Wave Propagation through Random Media*, Springer-Verlag, Berlin.

Saito, T., H. Sato, and M. Ohtake (2002). Envelope broadening of spherically outgoing waves in three-dimensional random media having power-law spectra, *J. Geophys. Res.* **107,** B5, 2089, doi 10.1029/2001JB000264.

Sato, H. (1977). Energy propagation including scattering effect: Single isotropic scattering approximation, *J. Phys. Earth* **25,** 27–41.

Sato, H., and M. C. Fehler (1998). *Seismic Wave Propagation and Scattering in the Heterogeneous Earth*, Springer-Verlag, New York.

Sens Schönfelder, C., and U. Wegler (2006). Radiative transfer theory for estimation of the seismic moment, *Geophys. J. Int.* **167,** 1363–1372.

Shang, T., and L. Gao (1988). Transport theory of multiple scattering and its application to seismic coda waves of impulsive source, *Sci. Sin. Ser. B* **31,** 1503–1514.

Singh, S. K., D. García, J. F. Pacheco, R. Valenzuela, B. K. Bansal, and R. S. Dattatrayam (2004). Q of the Indian Shield, *Bull. Seism. Soc. Am.* **94,** 1564–1570.

Talwani, P., and A. Gangopadhyay (2001). Tectonic framework of the Kachchh earthquake of 26 January 2001, *Seism. Res. Lett.* **72,** 336–345.

Van de Hulst, H. C. (1980). *Multiple Light Scattering*, Academic Press, New York.

Wang, J. H., and M. W. Huang (2004a). Displacement spectra of near-fault seismograms, 57-OSE-M139, in *AOGS Seminars*, July 5–9, 2004, Singapore.

Wang, J. H., and M. W. Huang (2004b). Can the Gutenberg-Richter's energy-magnitude relationship work for all earthquakes?, 57-OSE-M138, in *AOGS Seminars*, July 5–9, 2004, Singapore.

Watanabe, H. (1971). Determination of earthquake magnitude at regional distance in and near Japan, *Zisin* **24,** 189–200.

Wegler, U. (2003). Analysis of multiple scattering at Vesuvius Volcano, Italy, using data of the Tomo Ves active seismic experiment, *J. Volcanol. Geotherm. Res.* **128,** 45–63.

Wessel, P., and W. H. F. Smith (1995). New version of the Generic Mapping Tools released, *EOS Trans. AGU* **76,** 329.

Williamson, I. P. (1972). Pulse broadening due to multiple scattering in the interstellar medium, *Mon. Not. R. Astron. Soc.* **157,** 55–71.

Yoshimoto, K. (2000). Monte-Carlo simulation of seismogram envelopes in scattering media, *J. Geophys. Res.* **105,** no. B3, 6153–6161.

Zeng, Y., F. Su, and K. Aki (1991). Scattering wave energy propagation in a random isotropic scattering medium. I. Theory, *J. Geophys. Res.* **96,** 607–619.

National Geophysical Research Institute
Hyderabad 500007, India
(S.P.)

Department of Geophysics and Geology
University of Leipzig
D-04103 Leipzig, Germany
(U.W., M.K.)

Manuscript received 16 February 2006.